J Nanostruct 16(4): 5663-5675, Autumn 2026

RESEARCH PAPER

Evaluation of Silver Nanoparticle-Coated Catheters for Prevention of Biofilm Formation by Pseudomonas aeruginosa Clinical Isolates

Ahmed Zuhair Alwaeli [1] *, ***Thikra Ghaly AL-Timimi*** [2], ***Muslim M. M. Jassim*** [3], ***Zeyad Kadhim Oleiwi*** [4,5], ***Osama A. Mohsein*** [6,7]

[1] *Department of Microbiology, College of Medicine, University of Al-Ameed, Karbala, Iraq*

[2] *General Directorate of Education, Najaf, Iraq*

[3] *College of Science, University of Cordoba, Najaf 54001, Iraq*

[4] *Department of Pharmaceutical Chemistry, Faculty of Pharmacy, University of Kufa, Iraq*

[5] *Faculty of Pharmacy, University of Cordoba, Iraq*

[6] *Department of Medical Laboratory Techniques, College of Health and Medical Techniques, Northern Technical University, Kirkuk, Iraq*

[7] *Thi-Qar Health Directorate, Al Habbobi Teaching Hospital, Thi-Qar, Iraq*

ARTICLE INFO

Article History:
Received 09 June 2026
Accepted 17 September 2026
Published 01 October 2026

Keywords:
Antibiofilm activity
Biofilm formation
Catheter-associated infections
Pseudomonas aeruginosa
Silver nanoparticles

ABSTRACT

Pseudomonas aeruginosa readily forms antibiotic-resistant biofilms on catheter surfaces, highlighting the need for effective antimicrobial coatings such as silver nanoparticles. To evaluate the antibacterial and antibiofilm efficacy of silver nanoparticle-coated catheters against clinical *Pseudomonas aeruginosa* isolates and characterize the nanoparticles and coated surfaces using physicochemical techniques.An experimental laboratory-based study was conducted from January to August 2026 using 120 clinical samples from hospitalized patients with suspected catheter-associated infections. *Pseudomonas aeruginosa* was isolated using standard microbiological methods, followed by antimicrobial susceptibility and biofilm testing. Silver nanoparticles were green-synthesized, purified, and applied to silicone catheter segments by dip coating. AgNPs and coated surfaces were characterized using UV–Vis spectroscopy, XRD, FT-IR, SEM, and TEM. Antibiofilm efficacy was assessed by crystal-violet staining and viable bacterial counts. Data were analyzed using SPSS version 26. Among 120 clinical samples, 82 (68.3%) were culture-positive, yielding 46 *Pseudomonas aeruginosa* isolates, of which 34 (73.9%) exhibited biofilm-forming capacity. The highest resistance rate was observed for ceftazidime (63.0%), whereas meropenem showed the highest susceptibility (71.7%). The synthesized AgNPs had a mean particle size of 31.8 ± 5.6 nm and demonstrated stable surface deposition. AgNP-coated catheters significantly reduced biofilm biomass by 63.4% and viable bacterial attachment by 72.1% ($P<0.001$), accompanied by a marked reduction in strong biofilm formation from 55.9% to 17.6%. In conclusion, silver nanoparticle-coated catheters demonstrated substantial antibacterial and antibiofilm activity against clinical *Pseudomonas aeruginosa* isolates, significantly reducing biofilm biomass, viable bacterial attachment, and strong biofilm formation. These findings support AgNP-based catheter coatings as a promising strategy for limiting device-associated bacterial colonization and biofilm development.

How to cite this article
Zuhair Alwaeli A, Ghaly AL-Timimi T, M. Jassim MM, et al. Evaluation of Silver Nanoparticle-Coated Catheters for Prevention of Biofilm Formation by Pseudomonas aeruginosa Clinical Isolates. J Nanostruct, 2026; 16(4):5663-5675. DOI: 10.22052/JNS.2026.04.096

* *Corresponding Author Email: ahmed@alameed.edu.iq*

This work is licensed under the Creative Commons Attribution 4.0 International License.
To view a copy of this license, visit http://creativecommons.org/licenses/by/4.0/.

INTRODUCTION

Causing a significant problem in clinical practice today, catheter-associated infections continues to be one of the most relevant and critical healthcare-associated complications. The surfaces of medical devices like urinary catheters, vascular catheters and endotracheal tubes are ideal for microbial attachment, colonization, and development of biofilm that can lead to chronic infection, suboptimal therapeutic outcomes, extended hospital stays, and negative clinical outcomes[1, 2]. *Pseudomonas aeruginosa* is of special interest among bacterial pathogens associated with healthcare- and device-associated infections because of its opportunistic nature, metabolic adaptability, wide spectrum of virulence factors, and remarkable ability to acquire antimicrobial resistance [3].

Pseudomonas aeruginosa is an opportunistic and Gram-negative bacterium that can colonize biotic and abiotic surfaces. It has a large number of virulence factors such as exotoxins, elastases, proteases, pyocyanin, flagella, type IV pili, secretion systems, and interlinked quorum-sensing networks, which can help it bind to host tissues, destroy tissue, evade immune responses, and persist in the host [4]. *P. aeruginosa* has several important pathogenic properties, most notably the capacity to form biofilms on medical devices and host tissues [5]. These biofilms are organized microbial aggregates surrounded by a biofilm matrix that is secreted by the microorganisms themselves and contributes to bacterial resistance and persistence, as well as reduced susceptibility to antimicrobials and host immune defenses [6].

Biofilm formation significantly complicates the treatment of CAIs because bacteria in the biofilm are phenotypically tolerant and less sensitive to antimicrobial agents than planktonic bacteria [7]. Biofilm-associated infections can therefore become chronic, recurrent, and resistant to treatment with antimicrobial agents.

Furthermore, *P. aeruginosa* has several intrinsic, acquired and adaptive resistance mechanisms such as the production of β-lactamases, overexpression of multidrug efflux pumps, decreased outer membrane permeability, modification of the target site and acquisition of mobile resistance determinants [8]. Therefore, alternative antimicrobial and antibiofilm strategies have become increasingly important with the rise of multidrug-resistant *P. aeruginosa* in the clinical setting [9]. This represents a clinical need because *P. aeruginosa* is a member of the ESKAPE group of pathogens and is considered one of the most difficult pathogens to treat in modern clinical settings [10].

Nanotechnology has become an interdisciplinary area of major interest for medical, microbiological, biomaterials, diagnostic, and antimicrobial applications. Silver nanoparticles (AgNPs) are particularly interesting metallic nanomaterials due to their antimicrobial activity against a wide range of microorganisms and their unique physicochemical properties [11]. They are small and have a large surface-area-to-volume ratio, and their particle size, morphology, surface chemistry, and functionalization can be tuned to increase their interactions with microbial cells and biological surfaces [12]. Furthermore, the recent development of synthetic methods for the preparation and functionalization of AgNPs has broadened their potential biomedical applications, although the safety of these nanoparticles in biological systems still depends on their physicochemical properties, concentration, exposure conditions, and formulation [13].

The antibacterial action of silver nanoparticles is due to a number of partly overlapping mechanisms. They include interaction with and disruption of bacterial cell envelopes, release of biologically active silver ions, generation of reactive oxygen species (ROS), interference with proteins and respiratory enzymes, induction of oxidative stress and damage to intracellular components, such as nucleic acids [14]. Critically, AgNPs can also have antibiofilm activity through the inhibition of bacterial attachment, effects on extracellular polymeric substances (EPS), interference with biofilm development processes [15]. Experimental findings have shown the antimicrobial and antibiofilm activity of biologically synthesized AgNPs against *P. aeruginosa*, and these nanoparticles have been proposed as complementary antimicrobial agents against biofilm-forming bacteria [16]. In more recent studies, it has also been shown that the antibacterial activity of AgNPs can be extended to the attenuation of virulence factors and biofilm formation in *P. aeruginosa*, which are regulated by quorum sensing [17].

The use of silver nanoparticles on the surface of catheters has thus become a promising technique to minimize bacterial adhesion

CC BY

and biofilm formation. Antimicrobial agents incorporated into catheter coatings can act at the device–microorganism interface to offer local antimicrobial activity and can reduce microbial adhesion, an effect that cannot be achieved solely through systemic antimicrobial administration [18]. Experimental AgNP-containing hydrogel coatings have been shown to provide long-term silver release, as well as antibacterial and anti-adhesion properties on urinary catheter surfaces [19]. Surface modification is also believed to be a promising strategy to inhibit microbial colonization of catheter surfaces, as demonstrated by the development of advanced multilayer coatings incorporating silver and exhibiting significant antibiofilm properties [20].

Silver nanoparticles and catheter surfaces coated with these nanoparticles must be characterized in terms of their physicochemical properties, as nanoparticle parameters can directly affect their antimicrobial properties and biological behavior. The distribution and stability of the coating can also influence these properties. To verify the synthesis of AgNPs and characterize their structure, techniques such as UV–Visible spectroscopy, X-ray diffraction (XRD), Fourier-transform infrared spectroscopy (FT-IR), scanning electron microscopy (SEM), and transmission electron microscopy (TEM) are widely used [21].

Although the use of antimicrobial nanotechnology is becoming increasingly common, the number of studies that directly correlate the physicochemical characterization of AgNP coatings with their antibacterial and antibiofilm activity against clinical biofilm-forming *P. aeruginosa* isolates is still relatively small. Therefore, the present study aimed to evaluate the antibacterial and antibiofilm activities of silver nanoparticle-coated catheters against clinical isolates of *P. aeruginosa*. The study also aimed to determine the physicochemical characteristics of the prepared silver nanoparticles and catheter-coated surfaces using complementary physicochemical characterization methods, and to evaluate the potential of the prepared silver nanoparticles to reduce bacterial colonization and catheter-associated biofilm formation.

MATERIALS AND METHODS

Study Design and Clinical Samples

This experimental laboratory study was carried out from January to August 2026 to assess the efficacy of silver nanoparticle-coated catheters in inhibiting the ability of clinical isolates of *Pseudomonas aeruginosa* to form biofilm. One hundred and twenty clinical samples were collected from hospitalized patients who were suspected of having catheter-associated infections. Samples consisted of urine specimens, catheter tips, wound swabs, and respiratory secretions collected in a sterile manner and sent immediately to the microbiology laboratory for analysis.

Isolation and Identification of Pseudomonas aeruginosa

Clinical samples were cultured on blood agar, MacConkey agar, and cetrimide agar plates and grown aerobically at 37°C for 24–48 hours. All isolates were identified using standard microbiological techniques based on colony morphology, pigment production, the oxidase test, motility, citrate utilization, and the ability to grow at 42°C.

Antibiotic Susceptibility Testing

Antimicrobial susceptibility testing was carried out by the disk diffusion method on Mueller–Hinton (MH) agar, following the guidelines of the Clinical and Laboratory Standards Institute (CLSI). The antibiotics tested were ceftazidime, cefepime, ciprofloxacin, gentamicin, amikacin, piperacillin–tazobactam, and meropenem. MDROs were defined as isolates resistant to three or more classes of antimicrobial agents.

Detection of Biofilm Formation

The ability of the bacteria to form biofilm was determined by the crystal violet staining method in microplates. For a brief period, bacterial suspensions with an optical density of 0.5 McFarland were added to sterile 96-well microplates containing tryptic soy broth with 1% glucose and allowed to grow at 37°C for 24 hours. Wells were washed with phosphate-buffered saline (PBS), fixed with methanol, stained with crystal violet, and the OD was determined at 570 nm with a microplate reader. Biofilm intensity was categorized based on the optical density readings as weak, moderate, or strong.

Synthesis of Silver Nanoparticles

The green synthesis method was employed for the synthesis of silver nanoparticles (AgNPs). In brief, the plant powder (20 g) was placed in

CC BY

distilled water (200 mL) and boiled at 60 °C for 30 minutes to prepare the aqueous medicinal plant extract. Whatman No. 1 filter paper was used to filter the extract. For the synthesis of nanoparticles, 50 mL of plant extract was mixed with 50 mL of a 1 mM silver nitrate solution while stirring continuously at room temperature. A pale yellow to dark brown color change was observed, indicating the formation of silver nanoparticles. The synthesized nanoparticles were centrifuged at 12,000 rpm for 15 minutes, washed several times with distilled water and ethanol, dried at 70 °C, and stored for further analysis.

Preparation of Silver Nanoparticle-Coated Catheters

Commercial sterile silicone urinary catheters were divided into equal lengths and washed with sterile distilled water. AgNPs were dip-coated onto the catheter segments for 24 hours, and the segments were then allowed to dry at room temperature under sterile conditions. The coating procedure was repeated twice to improve nanoparticle adhesion and surface uniformity.

Characterization of Silver Nanoparticles and Coated Catheters

The synthesized silver nanoparticles and the coated catheter surface were analyzed using various techniques. UV–Visible spectroscopy was used to determine the surface plasmon resonance peak of AgNPs. X-ray diffraction (XRD) was used to identify the crystalline structure and purity of the nanoparticles. FT-IR spectroscopy was performed to identify the functional groups responsible for nanoparticle stabilization. The morphology of the nanoparticles and their distribution on the catheter surface were analyzed by scanning electron microscopy (SEM). To ascertain the size, aggregation, and ultrastructural morphology of the nanoparticles, transmission electron microscopy (TEM) was performed.

Evaluation of Antibiofilm Activity on Catheter Surfaces

P. aeruginosa biofilm-producing isolates were used to inoculate sterile coated and uncoated catheter segments in the biofilm growth chamber at 37°C for 24 hours. Catheter segments were then gently flushed with phosphate-buffered saline to remove non-adherent bacteria after incubation. The crystal violet staining method was used to quantify the biofilms formed on the surface of the catheters and OD values at 570 nm were taken.

Determination of Viable Bacterial Count on Catheter Surfaces

After biofilm formation, sections of the catheter were placed in sterile saline and vortexed for a few seconds to remove any bacterial cells that were attached. Serial dilutions were made and cultivated on nutrient agar plates. Colony-forming units (CFU/cm²) were counted after 24 hrs incubation at 37°C.

Statistical Analysis

Data were analyzed using SPSS version 26 (IBM Corporation, Armonk, NY, USA). Continuous variables were summarized as mean ± SD, while categorical variables were summarized as frequencies and percentages. For quantitative variables, an independent t-test was used to compare two groups, while one-way ANOVA followed by Tukey's post hoc test was used for comparisons among more than two groups. The chi-square test was used for categorical comparisons. A p-value of less than 0.05 was considered statistically significant.

Ethical Approval

All procedures in this study were conducted in compliance with ethical and biosafety guidelines, and the study protocol was approved by the

Table 1. Distribution of Clinical Bacterial Isolates and Biofilm-Producing *Pseudomonas aeruginosa* among the Examined Clinical Samples.

Parameter	No.	%
Total clinical samples	120	100
Positive bacterial culture	82	68.3
Pseudomonas aeruginosa isolates	46	56.1
Other bacterial isolates	36	43.9
Biofilm-producing *P. aeruginosa* isolates	34	73.9
Non-biofilm-producing isolates	12	26.1

CC BY

Human Ethics Committee. All participants gave informed consent, and clinical samples were collected.

RESULTS AND DISCUSSION

As presented in Table 1, the frequency of culture positivity, *P. aeruginosa* isolation, and biofilm-producing phenotypes among collected clinical specimens

A total of 120 clinical samples were collected, and 68.3% (82) were positive for bacterial culture. Forty-six (56.1%) positive cultures were due to P. aeruginosa, while other bacterial species accounted for 36 (43.9%). The *P. aeruginosa* isolates were high biofilm producers (34; 73.9%) and, 12 (26.1%) did not form biofilms.

Distribution of resistant and susceptible P. aeruginosa isolates across seven clinically relevant antimicrobial agents

As indicated in Table 2, the highest resistance rates were observed for ceftazidime, cefepime, and ciprofloxacin, at 63.0%, 58.7%, and 54.3%, respectively, followed by gentamicin (47.8%). In contrast, meropenem showed the highest level of antibacterial activity, with 71.7% of all isolates being susceptible, followed by amikacin (65.2%) and piperacillin–tazobactam (60.9%), suggesting that these agents retained relatively high activity against the isolates tested.

Characterization of Nanoparticle size, Surface Morphology, Zeta Potential, Coating Stability, and Time-Dependent Silver Release

As shown in Fig. 1, the UV–Vis spectrum exhibited a prominent absorption peak at approximately 435 nm (1.62 a.u.), attributed to the localized surface plasmon resonance (LSPR) of AgNPs, confirming their formation in the colloidal suspension. The broad absorption band may be associated with particle-size distribution and interparticle interactions.

The crystalline structure of the AgNPs was further examined by X-ray diffraction (XRD). As presented in Fig. 2, four prominent diffraction peaks were observed at 2θ values of approximately 38.12°, 44.32°, 64.45°, and 77.42°. These reflections were indexed to the (111), (200), (220), and (311) crystallographic planes, respectively, in agreement with the face-centered cubic (FCC) structure of metallic silver. The crystal structure of the silver nanoparticles corresponds to JCPDS reference code 04-0783, indicating the successful formation of the nanostructure.

As shown in Fig. 3, SEM images (A1–A3) illustrate the morphology of AgNPs, which were predominantly spherical to quasi-spherical in shape. Images (B1–B3) show the catheter surface

Table 2. Antimicrobial Susceptibility and Resistance Profiles of Clinical *Pseudomonas aeruginosa* Isolates Against Commonly Used Antibiotics.

Antibiotic	Resistant No. (%)	Sensitive No. (%)
Ceftazidime	29 (63.0)	17 (37.0)
Cefepime	27 (58.7)	19 (41.3)
Ciprofloxacin	25 (54.3)	21 (45.7)
Gentamicin	22 (47.8)	24 (52.2)
Amikacin	16 (34.8)	30 (65.2)
Piperacillin-tazobactam	18 (39.1)	28 (60.9)
Meropenem	13 (28.3)	33 (71.7)

Table 3. Physicochemical Characteristics, Surface Stability, and Silver Release Profile of Silver Nanoparticle-Coated Catheters Used in This Study.

Parameter	Result
Nanoparticle type	Silver nanoparticles
Coating method	Dip-coating technique
Mean AgNP size	31.8 ± 5.6 nm
Surface morphology	Uniform nanoparticle distribution
Zeta potential	−22.4 ± 3.2 mV
Coating stability after washing	87.6 ± 6.1%
Silver release after 24 h	0.42 ± 0.08 µg/mL
Silver release after 72 h	0.91 ± 0.13 µg/mL

after coating by dip-coating, revealing a relatively uniform nanoparticle distribution with some localized aggregation.

As presented in Fig. 4, TEM analysis confirmed the predominantly spherical morphology of AgNPs, with a mean particle size of 31.8 ± 5.6 nm. HRTEM and SAED patterns showed diffraction rings corresponding to the (111), (200), (220), and (311) planes, consistent with the face-centered cubic (FCC) structure of metallic silver.

As shown in Fig. 5, the FT-IR spectrum exhibited absorption bands at 3421 cm^{-1} (O–H stretching), 2924 cm^{-1} (aliphatic C–H stretching), 1632 cm^{-1} (C=O/amide-related vibrations), 1384 cm^{-1} (C-N

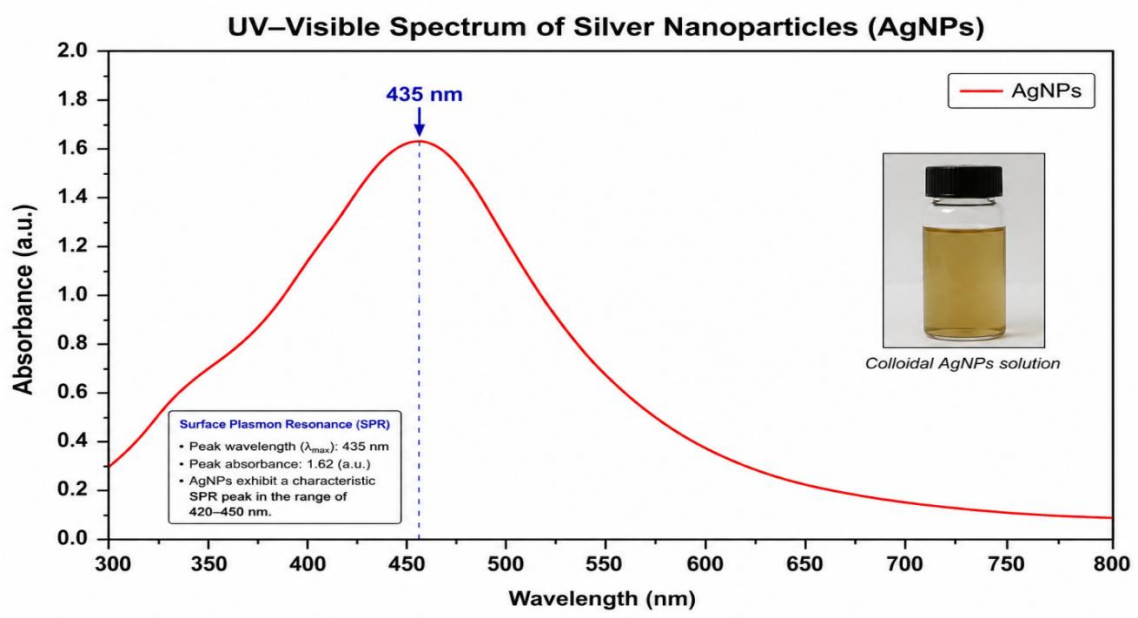


Fig. 1. UV–Visible absorption spectrum of AgNPs.

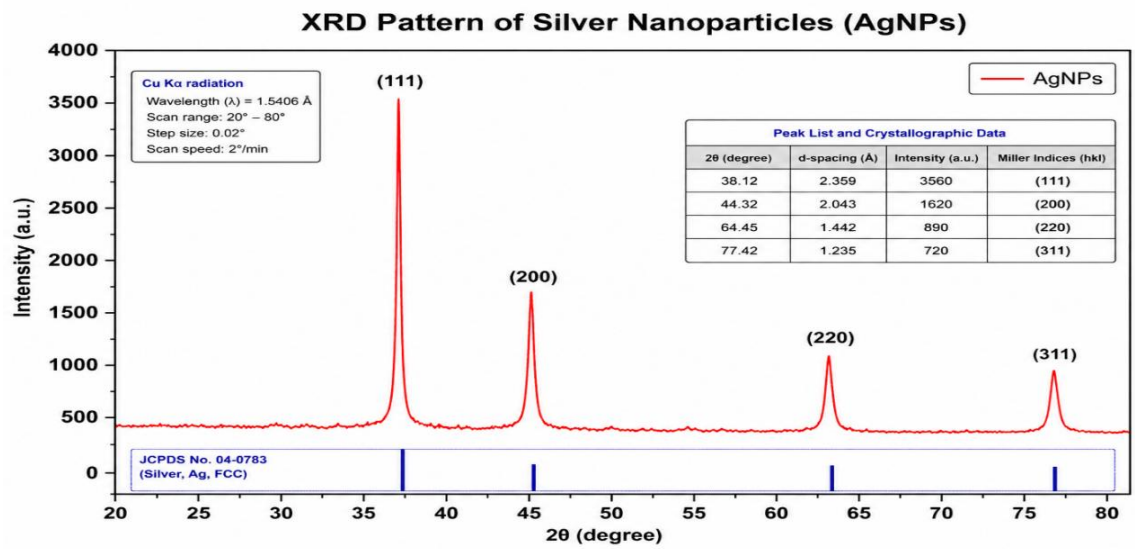


Fig. 2. X-ray diffraction (XRD) pattern of silver nanoparticles.

CC BY

stretching), and 1117 cm^{-1} (C–O stretching). The bands at 619 and 443 cm^{-1} associated with metal–oxygen (M–O) vibrations, while the band at 443 cm^{-1} may also be attributed to metal–nitrogen (M–N) vibrations.

Silver release increased from 0.42 ± 0.08 µg/mL at 24 h to 0.91 ± 0.13 µg/mL at 72 h, indicating continued silver accumulation in the release medium over time.

The zeta potential of −22.4 ± 3.2 mV indicated a negatively charged nanoparticle dispersion. The coating retained 87.6 ± 6.1% of its initial value after washing, suggesting substantial coating retention under the applied conditions, as summarized in Table 3.

Comparison of Biofilm Optical Density and Percentage Reduction Among Uncoated, AgNP-Coated, and Antibiotic-Coated Catheter Surfaces

The results in Table 4 indicate that treatment of the catheter surface led to significantly lower biofilm biomass than that on the uncoated catheter. Catheters coated with AgNPs had the lowest mean OD_{570} value (0.52 ± 0.18), representing a 63.4% reduction in biofilm formation compared with the control catheter ($P < 0.001$), while antibiotic-coated catheters showed a 51.4% reduction, with a mean OD_{570} of 0.69 ± 0.22 ($P < 0.001$).

Comparison of Viable Bacterial Counts and Colonization Reduction Among Uncoated, AgNP-Coated, and Antibiotic-Coated Catheter Surfaces

AgNP coating substantially reduced viable bacterial attachment from $6.8 \times 10^5 \pm 1.4 \times 10^5$ CFU/cm² on uncoated catheters to $1.9 \times 10^5 \pm 0.8 \times 10^5$ CFU/cm², representing a 72.1% reduction ($P<0.001$). In comparison, antibiotic coated-catheters showed a smaller reduction of 60.3%, with the viable count of $2.7 \times 10^5 \pm 1.1 \times 10^5$ CFU/cm² ($P<0.001$), as presented in Table 5.

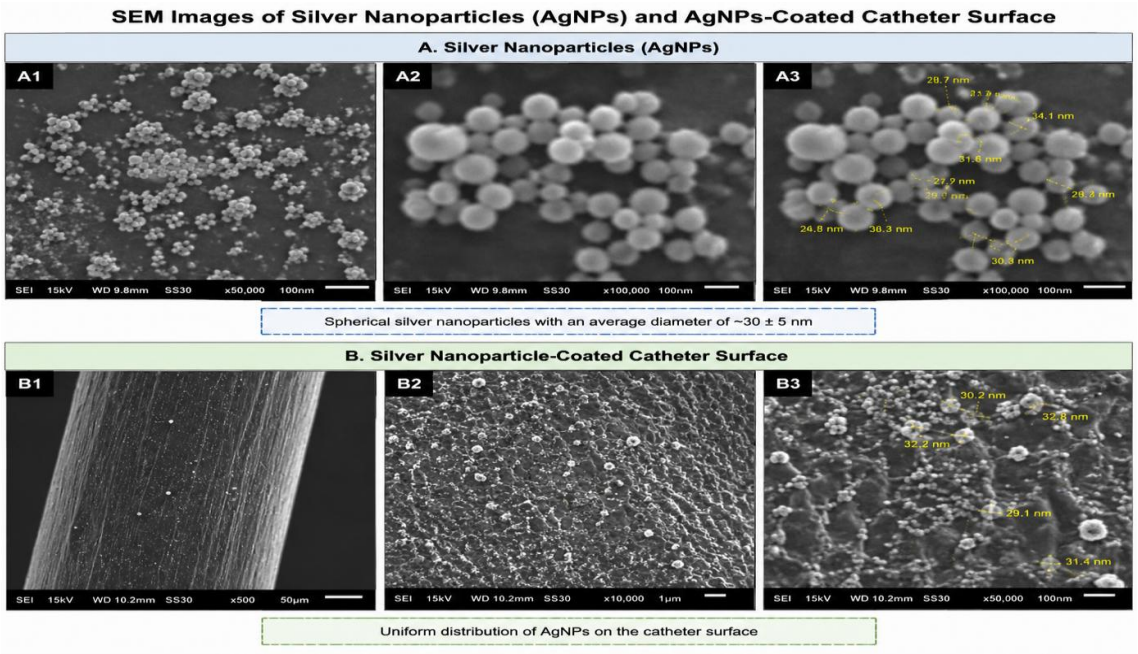


Fig. 3. SEM micrographs of silver nanoparticles and AgNP-coated catheter surface.

Table 4. Effect of Silver Nanoparticle-Coated Catheters on Biofilm Biomass Formation by Clinical *Pseudomonas aeruginosa* Isolates.

Catheter type	OD value at 570 nm Mean ± SD	Biofilm reduction %	p-value
Uncoated catheter	1.42 ± 0.31	—	—
Silver nanoparticle-coated catheter	0.52 ± 0.18	63.4%	<0.001
Antibiotic-coated catheter	0.69 ± 0.22	51.4%	<0.001

CC BY

Changes in Strong, Moderate, Weak, and Absent Biofilm Phenotypes Following Exposure to AgNP-Coated Catheter Surfaces

Biofilm formation shifted markedly toward less intense phenotypes following AgNP coating. The percentage of strong biofilm producers decreased from 55.9% to 17.6% (P<0.001), while weak biofilm formation increased from 14.7% to 38.2% (P = 0.028), and the complete absence of biofilm formation increased from 0% to 17.6% (P = 0.011) between the two groups. There was no significant difference in the proportion of isolates exhibiting moderate biofilm formation between the two groups (29.4% vs. 26.5%; P = 0.791) which summarized in Table 6.

In the present study, microbiological and physicochemical evidence is presented to support the potential of AgNP-coated catheters to inhibit colonization by clinical *Pseudomonas aeruginosa* isolates and biofilm formation. *P. aeruginosa* was cultured from 46 (56.1%) of the 82 culture-positive specimens, with 34 (73.9%) of the isolates being capable of forming biofilms. Such a high proportion is biologically plausible, as *P. aeruginosa* is known to have a complex biofilm formation mechanism that includes early surface adhesion, flagella and pili, extracellular polymeric substances, alginate, Pel and Psl polysaccharides, extracellular DNA, and quorum sensing-mediated maturation [5]. Other clinical studies have also shown high rates of biofilm production by *P. aeruginosa*. Azab et al. found that approximately 80% of clinical isolates formed biofilms, which is fairly close to the 73.9% found in the present study [22]. Additionally, Hemmati et al. reported a significant correlation between multidrug resistance and phenotypic and genotypic features associated with biofilm production in clinical isolates of *P. aeruginosa* [23]. All these observations contribute to the understanding that biofilm production is a key survival phenotype in clinical *P. aeruginosa* and not a laboratory artifact.

However, the capacity to form a biofilm varies widely across published studies. For instance, there are reports of a decreased proportion of biofilm producers or variation in the distribution of weak, moderate, or strong biofilm producers, while highly selected isolates from burn or chronic

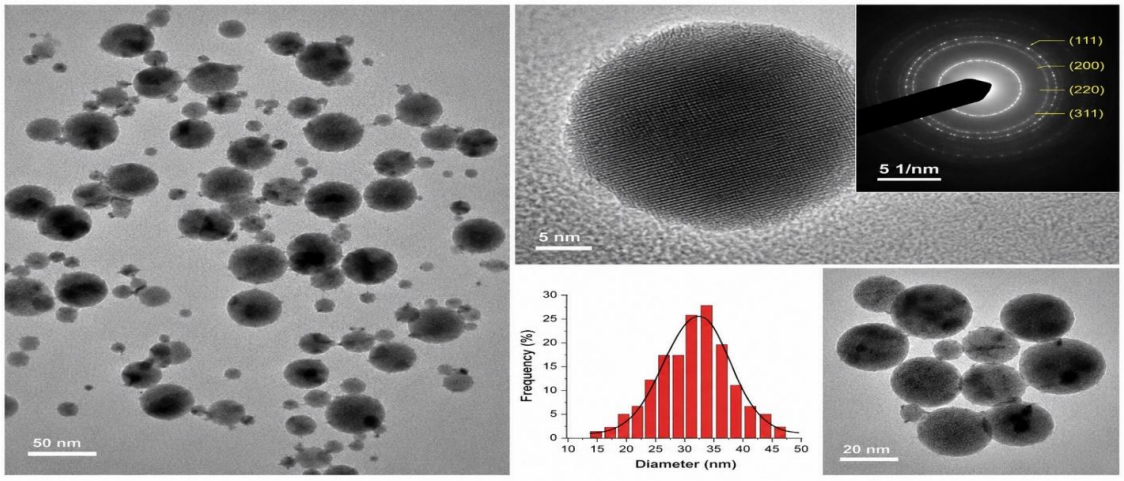


Fig. 4. TEM images of silver nanoparticles.

Table 5. Effect of Silver Nanoparticle Coating on Viable *Pseudomonas aeruginosa* Attachment to Catheter Surfaces.

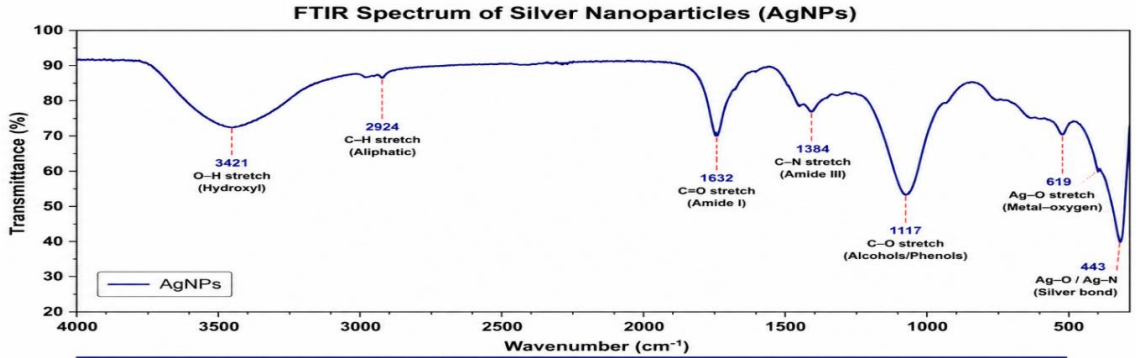
Catheter type	Bacterial count CFU/cm² Mean ± SD	Reduction compared with control	p-value
Uncoated catheter	$6.8 \times 10^5 \pm 1.4 \times 10^5$	—	—
Silver nanoparticle-coated catheter	$1.9 \times 10^5 \pm 0.8 \times 10^5$	72.1%	<0.001
Antibiotic-coated catheter	$2.7 \times 10^5 \pm 1.1 \times 10^5$	60.3%	<0.001

CC BY

wound infections have yielded unusually high frequencies [24, 25]. These discrepancies do not necessarily conflict with the results of the present study. They may reflect variations in anatomical origin, length of hospital stay, previous exposure to antimicrobial agents, bacterial genotype, disease severity, and local infection control practices. Methodological differences should also be considered because crystal violet microtiter assays measure attached biomass, not necessarily viable organisms, whereas other methods can provide estimates of metabolic activity, viable counts, or biofilm architecture. The incubation period, culture media, and inoculum concentration, as well as the definition of a biofilm and the substrate used, can therefore lead to varying estimates of biofilm prevalence [5, 23].

Further antimicrobial susceptibility testing confirms the therapeutic difficulties posed by the isolates studied. The highest resistance rates were observed for ceftazidime (63.0%), cefepime (58.7%), and ciprofloxacin (54.3%), while meropenem and amikacin showed greater activity, with susceptibility rates of 71.7% and 65.2%, respectively. The high levels of cephalosporin and fluoroquinolone resistance are typical of the resistance patterns currently observed in *P. aeruginosa*, which is known to develop a multitude of resistance mechanisms, such as AmpC production, acquired β-lactamases, mutations in porins, overexpression of multidrug efflux systems, target mutations, and acquisition of mobile resistance determinants [8, 26]. Biofilm growth also exacerbates this issue by limiting antimicrobial agent penetration, decreasing bacterial metabolic activity, promoting the formation of persister cells, and inducing stress responses and adaptive mechanisms within biofilms [27].

However, when compared region-wise, there are some quantitative differences. In a study of *P. aeruginosa* isolates from Basra, Iraq, Alkhulaifi and Mohammed reported that 98.95% were resistant to ceftazidime, 75.8% to cefepime, 71.6% to ciprofloxacin, and 68.4% to meropenem [28]. The values are much higher than those in the present study, which had the following corresponding values of 63.0%, 58.7%, 54.3%, and



Peak Position (cm⁻¹)	Functional Group	Vibrational Mode	Possible Origin / Assignment
3421	O–H	Stretching	Hydroxyl groups, adsorbed water, phytochemicals
2924	C–H	Stretching	Aliphatic C–H (–CH_2, –CH_3)
1632	C=O	Stretching	Amide I / Carbonyl groups from proteins or polyphenols
1384	C–N	Stretching	Amide III / Amino groups
1117	C–O	Stretching	Alcohols, phenols, ethers, or C–O–C groups
619	Ag–O	Stretching	Silver–oxygen interaction (Ag–O bond)
443	Ag–O / Ag–N	Stretching	Metal–oxygen / Metal–nitrogen vibration (Silver bond)

Fig. 5. FT-IR spectrum of silver nanoparticles.

Table 6. Distribution of *Pseudomonas aeruginosa* Biofilm Intensity on Uncoated and Silver Nanoparticle-Coated Catheter Surfaces.

Biofilm intensity	Uncoated catheter No. (%)	AgNP-coated catheter No. (%)	p-value
Strong biofilm	19 (55.9)	6 (17.6)	<0.001
Moderate biofilm	10 (29.4)	9 (26.5)	0.791
Weak biofilm	5 (14.7)	13 (38.2)	0.028
No biofilm	0 (0.0)	6 (17.6)	0.011

28.3%. However, the present study also revealed that meropenem had comparatively good activity, which is consistent with the results of Hemmati et al., who found that meropenem was one of the more active agents against some of the clinical isolates of P. aeruginosa, although the overall level of MDR was [23]. This geographical variability can be attributed to varying antibiotic use, physicians' prescribing habits, antibiotic stewardship, patient demographics, hospital wards, infection control pressure, and local dissemination of high-risk resistant clones. The difference should therefore be considered as an example of the dynamic and geographically heterogeneous resistome of *P. aeruginosa* [8, 26] and not as a result of inconsistent laboratory performance.

The physicochemical findings support the evidence obtained using the other methods and indicate that the AgNP coating was successfully prepared. The mean particle size was 31.8 ± 5.6 nm, with a zeta potential of −22.4 ± 3.2 mV and coating retention of 87.6 ± 6.1% after washing. In addition, silver release increased from 0.42 ± 0.08 µg/mL at 24 h to 0.91 ± 0.13 µg/mL at 72 h. This is important because antimicrobial efficacy depends not only on the presence of elemental silver but also on particle size, surface chemistry, aggregation state, coating properties, and the amount of available Ag^+ released from the particles [12, 29]. The observed release profile may therefore influence both the initial burst release and the duration of local antimicrobial activity.

As shown in Fig. 1, the UV–Visible spectrum exhibited a characteristic surface plasmon resonance (SPR) band at approximately 435 nm, which provides optical evidence for the formation of AgNPs. Surface plasmon resonance in this spectral range has been described in recent reviews on AgNP characterization, with the SPR position depending on particle size, morphology, aggregation, dielectric environment, and the surface-capping molecules of the nanoparticles [29, 30]. Thus, small deviations from the observed wavelength and from the ranges reported elsewhere should be considered normal and not necessarily indicative of unsuccessful synthesis. Instead, they may reflect differences in the chemical microenvironment surrounding the nanoparticles.

Fig. 2 shows the XRD analysis, which confirmed the crystalline structure of the AgNPs, with diffraction patterns consistent with the face-centered cubic (FCC) crystal structure of metallic silver. The characteristic reflections of AgNPs corresponding to the (111), (200), (220), and (311) planes have been widely reported [29, 30]. The current results are thus consistent with previously reported structural characteristics of metallic silver nanoparticles. Variations in peak width or intensity among studies may be related to crystallite size, lattice strain, precursor concentration, reaction temperature, reaction duration, or the type of reducing or capping compounds used. Therefore, the XRD results should be correlated with TEM and SEM findings rather than being regarded as the sole criteria for evaluating nanoparticle quality.

As illustrated in Figure 3, SEM showed relatively uniform deposition of AgNPs throughout the length of catheter with minimal aggregation. This is a crucial discovery, because the uniformity of the coating is important for the area of direct contact between bacteria and the nanoparticles and is important for the release of silver and availability of unprotected surfaces for the initial adsorption of microbes. A similar successful grafting of silver nano-particles with a green synthesis method on urinary catheter surface was demonstrated by Lethongkam et al. which showed significant inhibition of microbial migration, adhesion, and biofilm formation [31]. Al Rugaie et al. also demonstrated that polymer-stabilized metallic nanoparticle coatings could be used to inhibit biofilm growth on urinary catheter surfaces [32]. The moderate aggregation observed in the present SEM images is not surprising, as metallic nanoparticles have high surface energy and may cluster during drying, coating, or even storage. Most importantly, the limited aggregation did not completely eliminate the biological activity observed in the subsequent assays.

The TEM image showed mostly spherical nanoparticles with an average size ranging from 20 to 40 nm (Fig. 4). The morphology is particularly significant in relation to antibacterial effects. Kumar et al. synthesized AgNPs using plant extracts, with an average diameter of approximately 30 nm, and showed that the synthesized AgNPs effectively inhibited *P. aeruginosa* biofilm formation and the expression of quorum-sensing-regulated virulence factors [33]. This similarity in particle size supports the biological plausibility of the present results. Conversely, Tabassum et al. obtained AgNPs with significantly larger average particle sizes, yet they still found strong antibiofilm and

CC BY

antivirulence properties associated with the AgNPs [17]. Therefore, although smaller particle sizes could improve surface interactions and Ag^+ release, antimicrobial performance cannot be attributed solely to particle size; it also depends on functionalization, surface charge, corona composition, dispersion, and exposure conditions.

The functional groups identified via FT-IR analysis were in agreement with the presence of O–H, C=O, and C–N-containing compounds on the surface of the nanoparticles, as shown in Fig.5. Similar results are consistent with the use of biological molecules as reducing and capping agents in green synthesis of nanoparticles. Thomas et al. highlighted the potential of phytochemicals with hydroxyl, carbonyl, amine, and other functional groups to reduce Ag+ and stabilize the formed AgNPs [13]. The variations in the FT-IR spectra of the current AgNP preparation and the other green-synthesized AgNP preparations can be reasonably attributed to the differences in the composition of the biological extract and the extraction process, as well as the reaction pH, temperature, and purification of the nanoparticles. Therefore, the FT-IR results should be treated as being indicative of surface-associated chemical functionalities, and not as evidence for any single chemical compound. A significant decrease in catheter-associated biofilm was the most significant functional observation. The optical density of the mean crystal violet was reduced from 1.42 ± 0.31 to 0.52 ± 0.18 after the coating of AgNP, a 63.4% reduction ($P<0.001$). Importantly, this drop was more than that seen in the antibiotic-coated comparator (51.4%). This result is in line with that of Goda et al., which showed significant inhibition of the bacterial biofilm growth on urinary catheters functionalized with the green-synthesized AgNPs [34]. They are also bolstered by Lethongkam et al., who reported that microbial adhesion, migration, and biofilm formation were inhibited in an environment that simulated the urinary tract using an AgNP-coated Foley catheter [31]. In recent years, hydrogel coatings containing AgNPs have shown high antibacterial and anti-adhesive properties, both on the external and internal surface of the catheter [19].

The extent of inhibition observed in the present study should be evaluated in the context of the substantial methodological variation among nanoparticle studies. Other investigations have reported higher antibiofilm activity than the 63.4% observed in the present study, whereas others have reported more moderate results. In the case of engineered or conjugated nanoparticles, for instance, the antimicrobial activity of silver can be enhanced by the addition of anti-adhesive polymers, biosurfactants, chitosan, or other functional molecules [19, 35]. On the other hand, reduced inhibition may occur in cases of nanoparticle aggregation, insufficient silver-ion release, incomplete coating, or the use of bacterial populations comprising highly adhesive clinical strains. Differences in biofilm maturity and assay endpoints are also crucial: inhibition of initial adhesion is typically more easily achieved than the eradication of mature biofilms with dense extracellular matrices.

The antimicrobial properties observed may be due to several complementary mechanisms. AgNPs can interact with bacterial envelopes, alter membrane permeability, affect membrane potential, generate reactive oxygen species, damage proteins and intracellular macromolecules, and release Ag^+ ions that can disrupt essential enzymatic processes [12, 15]. Exposure to AgNPs may also disrupt quorum sensing and inhibit the expression of virulence factors, including pyocyanin production, protease activity, motility, and genes involved in biofilm formation in *P. aeruginosa*. Kumar et al. showed the anti-quorum-sensing activity of phyto-synthesized AgNPs with a size of approximately 30 nm [33], while Tabassum et al. reported the inhibition of genes associated with virulence and biofilm formation [17]. Abo Kamer et al. also found that AgNPs were effective in inhibiting the growth of MDR and XDR clinical isolates of *P. aeruginosa* and enhanced the inhibitory effects of some antibiotics against these strains [36]. The present phenomenological results are supported by these observations, which provide mechanistic information.

The effect was not restricted to reduced crystal-violet-stained biomass and is supported by the viable-count assay. The bacteria were reduced by 72.1% from 6.8×10^5 CFU/cm² on uncoated catheters to 1.9×10^5 CFU/cm² on surfaces coated with AgNP ($P<0.001$). The reduction in the antibiotic-coated catheter was only 60.3%. This is significant as crystal violet measures both cells and extracellular matrix, while viable counting only measures culturable bacteria. The levels of agreement between these two independent endpoints thus indicate that the AgNP coating

CC BY

also inhibited the growth of surface biomass and the viable attached bacteria. The same decrease in CAC has been reported when using polymer coatings stabilized by nanoparticles and/or AgNP materials in catheters [19, 32].

A change in the distribution of the biofilm categories is also a good indicator of biological effectiveness. The percentage of strong biofilm formation decreased significantly from 55.9% with uncoated catheters to 17.6% with AgNP-coated catheters, and the percentages of weak or absent biofilm increased significantly. This indicates that the coating was not only able to cause a small quantitative change in biomass, but it also changed the distribution of biofilm development as a whole. This effect was similar to interference with the early attachment, and microcolony-development stages. Rahman et al. also showed that the AgNPs coupled with surfactin had significant antibacterial and antibiofilm properties against the drug-resistance *P. aeruginosa* [35]. Xia et al. also reported good antibacterial and antibiofilm activity of biosynthesized AgNPs, but the antibacterial activity was not consistent with respect to the concentration and experimental conditions [15].

Another useful outcome of the experiment is the sequential silver elution from the catheter. Cai et al showed that the coating of the hydrogel catheter with AgNP can lead to the sustained release of AgNPs/Ag^{+} and correlate the release with the prolonged antibacterial activity of the coating [19]. The release profile observed at 72 h in the current study is thus in line with the concept of sustained release. However, releasing the maximum amount of silver is not always advantageous, as host-cell compatibility and possible silver toxicity should be taken into account in relation to antimicrobial performance. Modern reviews highlight the critical role of dose, particle size, surface coating, exposure time, and the biological system studied in determining the effects of AgNPs [13, 37]. Therefore, it can be said that the present release profile is promising from an antimicrobial point of view, but it still needs to be investigated through dedicated cytocompatibility, hemocompatibility, and long-term release studies prior to clinical application.

CONCLUSION

Overall, the present results showed that the biomass of *P. aeruginosa* biofilm, the number of viable attached bacteria, and the incidence of strong biofilm formation were significantly decreased on the catheter surface coated with AgNPs under the studied in vitro conditions. The agreement among the findings obtained using UV–Visible spectroscopy, XRD, SEM, TEM, FT-IR, silver release, and crystal-violet assays and those obtained from the viable-count analysis further supports the internal consistency of the results. When comparing the results with those from the literature, the differences can easily be explained by variations in size, functionalization, coating density and stability, silver ion release, bacterial genotype, clinical origin, growth medium, biofilm development, and experimental endpoints. However, the findings should not yet be viewed as proof that the use of AgNP-coated catheters can decrease the rates of CAI in patients. Dynamic flow models with artificial or human urine, mature and polymicrobial biofilms, repeated-measures testing of silver release, mammalian-cell cytotoxicity and hemocompatibility testing, and finally, controlled in vivo and clinical testing should be conducted before AgNP-coated catheters are introduced into routine clinical use.

CONFLICT OF INTEREST

The authors declare that there is no conflict of interests regarding the publication of this manuscript.

REFERENCES

1. Mishra A, Aggarwal A, Khan F. Medical Device-Associated Infections Caused by Biofilm-Forming Microbial Pathogens and Controlling Strategies. Antibiotics. 2024;13(7):623.
2. Bouhrour N, Nibbering PH, Bendali F. Medical Device-Associated Biofilm Infections and Multidrug-Resistant Pathogens. Pathogens. 2024;13(5):393.
3. Qin S, Xiao W, Zhou C, Pu Q, Deng X, Lan L, et al. Pseudomonas aeruginosa: pathogenesis, virulence factors, antibiotic resistance, interaction with host, technology advances and emerging therapeutics. Signal Transduction and Targeted Therapy. 2022;7(1).
4. Chadha J, Harjai K, Chhibber S. Revisiting the virulence hallmarks of Pseudomonas aeruginosa: a chronicle through the perspective of quorum sensing. Environ Microbiol. 2021;24(6):2630-2656.
5. Tuon FF, Dantas LR, Suss PH, Tasca Ribeiro VS. Pathogenesis of the Pseudomonas aeruginosa Biofilm: A Review. Pathogens. 2022;11(3):300.
6. Miranda SW, Asfahl KL, Dandekar AA, Greenberg EP. Pseudomonas aeruginosa Quorum Sensing. Advances in Experimental Medicine and Biology: Springer International Publishing; 2022. p. 95-115. http://dx.doi.org/10.1007/978-3-031-08491-1_4
7. Zhao Y, Xu H, Wang H, Wang P, Chen S. Multidrug resistance in Pseudomonas aeruginosa: genetic control mechanisms and

therapeutic advances. Molecular Biomedicine. 2024;5(1).
8. Sendra E, Fernández-Muñoz A, Zamorano L, Oliver A, Horcajada JP, Juan C, et al. Impact of multidrug resistance on the virulence and fitness of Pseudomonas aeruginosa: a microbiological and clinical perspective. Infection. 2024;52(4):1235-1268.
9. Schwartz B, Klamer K, Zimmerman J, Kale-Pradhan PB, Bhargava A. Multidrug Resistant Pseudomonas aeruginosa in Clinical Settings: A Review of Resistance Mechanisms and Treatment Strategies. Pathogens. 2024;13(11):975.
10. Miller WR, Arias CA. ESKAPE pathogens: antimicrobial resistance, epidemiology, clinical impact and therapeutics. Nature Reviews Microbiology. 2024;22(10):598-616.
11. Essa SH, Mohammad SQ, Kadhum DA, Jalil IS. Effectiveness of silver nanoparticles as antibacterial agents with natural wound healing cream with extracted Aloe vera gel. Regulatory Mechanisms in Biosystems. 2024;15(4):821-825.
12. Tripathi N, Goshisht MK. Recent Advances and Mechanistic Insights into Antibacterial Activity, Antibiofilm Activity, and Cytotoxicity of Silver Nanoparticles. ACS Applied Bio Materials. 2022;5(4):1391-1463.
13. Thomas S, Gonsalves RA, Jose J, Zyoud SH, Prasad AR, Garvasis J. Plant-based synthesis, characterization approaches, applications and toxicity of silver nanoparticles: A comprehensive review. J Biotechnol. 2024;394:135-149.
14. More PR, Pandit S, Filippis AD, Franci G, Mijakovic I, Galdiero M. Silver Nanoparticles: Bactericidal and Mechanistic Approach against Drug Resistant Pathogens. Microorganisms. 2023;11(2):369.
15. Xia F, Tao X, Wang H, Shui J, Min C, Xia Y, et al. Biosynthesis of Silver Nanoparticles Using the Biofilm Supernatant of Pseudomonas aeruginosa PA75 and Evaluation of Their Antibacterial, Antibiofilm, and Antitumor Activities. International Journal of Nanomedicine. 2023;Volume 18:2485-2502.
16. Esfahani MB, Khodavandi A, Alizadeh F, Bahador N. Antibacterial and Anti-Biofilm Activities of Microbial Synthesized Silver and Magnetic Iron Oxide Nanoparticles Against Pseudomonas aeruginosa. IEEE Trans NanoBiosci. 2023;22(4):956-966.
17. Tabassum N, Khan F, Jeong G-J, Jo D-M, Kim Y-M. Silver nanoparticles synthesized from Pseudomonas aeruginosa pyoverdine: Antibiofilm and antivirulence agents. Biofilm. 2024;7:100192.
18. Ferreres G, Ivanova K, Torrent-Burgués J, Tzanov T. Multimodal silver-chitosan-acylase nanoparticles inhibit bacterial growth and biofilm formation by Gram-negative Pseudomonas aeruginosa bacterium. Journal of Colloid and Interface Science. 2023;646:576-586.
19. Cai Y, Yang H, Li J, Gu R, Dong Y, Zhao Q, et al. Antibacterial AgNPs-PAAm-CS-PVP nanocomposite hydrogel coating for urinary catheters. Eur Polym J. 2023;196:112260.
20. Bose S, Kang M, Jung S, Kim M, Yoon C, Ranganathan P, et al. Hierarchical silver-tannic acid hydrophobic coating via layer-by-layer assembly for antibiofilm applications on urinary catheters. Materials Today Bio. 2026;37:102775.
21. Sadia SI, Shishir MKH, Ahmed S, Alam MA, Al-Reza SM, Afrin S, et al. Green synthesis of crystalline silver nanoparticle by bio-mediated plant extract: A critical perspective analysis. Nano-Structures and Nano-Objects. 2024;39:101272.
22. Rehab EF, Samar MS, Amro MH, Marwa MA. Molecular detection of different virulence factors genes harbor pslA, pelA, exoS, toxA and algD among biofilm-forming clinical isolates of Pseudomonas aeruginosa. Cellular and Molecular Biology. 2023;69(5):32-39.
23. Hemmati J, Nazari M, Ahmadi A, Bayati M, Jalili M, Taheri M, et al. In vitro evaluation of biofilm phenotypic and genotypic characteristics among clinical isolates of Pseudomonas aeruginosa in Hamadan, West of Iran. J Appl Genet. 2023;65(1):213-222.
24. Chimi LY, Noubom M, Bisso BN, Singor Njateng GS, Dzoyem JP. Biofilm Formation, Pyocyanin Production, and Antibiotic Resistance Profile of Pseudomonas aeruginosa Isolates from Wounds. Int J Microbiol. 2024;2024(1).
25. Ganjo AR, Ali FA, Aka ST, Hussen BM, Smail SB. Diversity of biofilm-specific antimicrobial resistance genes in Pseudomonas aeruginosa recovered from various clinical isolates. Iranian Journal of Microbiology. 2023.
26. Fernández-Billón M, Llambías-Cabot AE, Jordana-Lluch E, Oliver A, Macià MD. Mechanisms of antibiotic resistance in Pseudomonas aeruginosa biofilms. Biofilm. 2023;5:100129.
27. Thöming JG, Häussler S. Pseudomonas aeruginosa Is More Tolerant Under Biofilm Than Under Planktonic Growth Conditions: A Multi-Isolate Survey. Frontiers in Cellular and Infection Microbiology. 2022;12.
28. Alkhulaifi ZMM, Mohammed KAS. Prevalence and molecular analysis of antibiotic resistance of Pseudomonas aeruginosa isolated from clinical and environmental specimens in Basra, Iraq. Iranian Journal of Microbiology. 2023.
29. Duman H, Eker F, Akdaşçi E, Witkowska AM, Bechelany M, Karav S. Silver Nanoparticles: A Comprehensive Review of Synthesis Methods and Chemical and Physical Properties. Nanomaterials. 2024;14(18):1527.
30. Magdy G, Aboelkassim E, Abd Elhaleem SM, Belal F. A comprehensive review on silver nanoparticles: Synthesis approaches, characterization techniques, and recent pharmaceutical, environmental, and antimicrobial applications. Microchem J. 2024;196:109615.
31. Lethongkam S, Paosen S, Bilhman S, Dumjun K, Wunnoo S, Choojit S, et al. Eucalyptus-Mediated Synthesized Silver Nanoparticles-Coated Urinary Catheter Inhibits Microbial Migration and Biofilm Formation. Nanomaterials. 2022;12(22):4059.
32. Rugaie OA, Abdellatif AAH, El-Mokhtar MA, Sabet MA, Abdelfattah A, Alsharidah M, et al. Retardation of Bacterial Biofilm Formation by Coating Urinary Catheters with Metal Nanoparticle-Stabilized Polymers. Microorganisms. 2022;10(7):1297.
33. Kumar S, Paliya BS, Singh BN. Superior inhibition of virulence and biofilm formation of Pseudomonas aeruginosa PAO1 by phyto-synthesized silver nanoparticles through anti-quorum sensing activity. Microb Pathog. 2022;170:105678.
34. Goda RM, El-Baz AM, Khalaf EM, Alharbi NK, Elkhooly TA, Shohayeb MM. Combating Bacterial Biofilm Formation in Urinary Catheter by Green Silver Nanoparticle. Antibiotics. 2022;11(4):495.
35. Rahman L, Sarwar Y, Khaliq S, Inayatullah, Abbas W, Mobeen A, et al. Surfactin-Conjugated Silver Nanoparticles as an Antibacterial and Antibiofilm Agent against Pseudomonas aeruginosa. ACS Applied Materials and Interfaces. 2023;15(37):43321-43331.
36. Kamer AMA, El Maghraby GM, Shafik MM, Al-Madboly LA. Silver nanoparticle with potential antimicrobial and antibiofilm efficiency against multiple drug resistant, extensive drug resistant Pseudomonas aeruginosa clinical isolates. BMC Microbiol. 2024;24(1).
37. Meher A, Tandi A, Moharana S, Chakroborty S, Mohapatra SS, Mondal A, et al. Silver nanoparticle for biomedical applications: A review. Hybrid Advances. 2024;6:100184.

CC BY